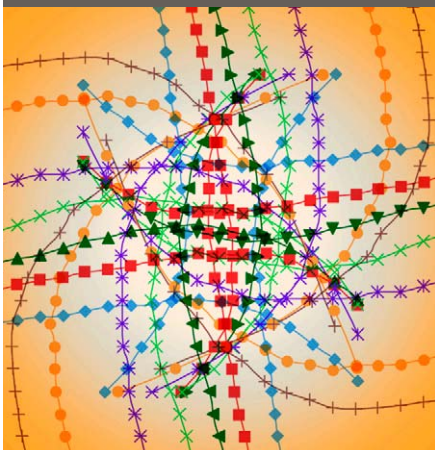


Yuxin Wu*
Susan S. Hubbard
Craig Ulrich
Stan D. Wulfschleger



Remote monitoring of freeze–thaw transition of arctic soils using the complex resistivity method was simulated in column studies. Our results revealed the sensitivity of this method to freeze–thaw transition and its potential for monitoring freeze–thaw processes in the arctic region that are critical to global carbon cycle and climate change.

Y. Wu, S. S. Hubbard, and C. Ulrich, Lawrence Berkeley National Lab., Berkeley, CA 94720; S. D. Wulfschleger, Oak Ridge National Lab., Oak Ridge, TN 37831. *Corresponding author (YWu3@lbl.gov)

Vadose Zone J.
doi:10.2136/vzj2012.0062
Received 1 May 2012.

© Soil Science Society of America
5585 Guilford Rd., Madison, WI 53711 USA.
All rights reserved. No part of this periodical may be reproduced or transmitted in any form or by any means, electronic or mechanical, including photocopying, recording, or any information storage and retrieval system, without permission in writing from the publisher.

Remote Monitoring of Freeze–Thaw Transitions in Arctic Soils Using the Complex Resistivity Method

Our ability to monitor freeze–thaw transitions is critical to developing a predictive understanding of biogeochemical transitions and carbon dynamics in high latitude environments. In this study, we conducted laboratory column experiments to explore the potential of the complex resistivity method for monitoring the freeze–thaw transitions of the arctic permafrost soils. Samples for the experiment were collected from the upper active layer of Gelisol soils at the Barrow Environmental Observatory (BEO) in Barrow, Alaska. Freeze–thaw transitions were induced through exposing the soil column to controlled temperature environments at 4 and -20°C . Complex resistivity and temperature measurements were collected regularly during the freeze–thaw transitions using electrodes and temperature sensors installed along the column. During the experiments, over two orders of magnitude of resistivity variations were observed when the temperature was increased or decreased between -20 and 0°C . Smaller resistivity variations were also observed during the isothermal thawing or freezing processes that occurred near 0°C . Single frequency electrical phase response and imaginary conductivity at 1 Hz were found to be exclusively related to the unfrozen water in the soil matrix, suggesting that these geophysical attributes can be used as a proxy for the monitoring of the onset and progression of the freeze–thaw transitions. Spectral electrical responses and fitted Cole–Cole parameters contained additional information about the freeze–thaw transition affected by the soil grain size distribution. Specifically, a shift of the observed spectral response to lower frequency was observed during the isothermal thawing process, which we interpret to be due to sequential thawing, first from fine particles and then to coarse particles within the soil matrix. Our study demonstrates the potential of the complex resistivity method for remote monitoring of freeze–thaw transitions in arctic soils. Although conducted at the laboratory scale, this study provides the foundation for exploring the potential of the complex resistivity signals for monitoring spatiotemporal variations of freeze–thaw transitions over field-relevant scales.

Abbreviations: BEO, Barrow Environmental Observatory; DC, direct current; EDL, electrical double layer; ERT, electrical resistivity tomography; IP, induced polarization

Approximately 1.7×10^{12} tons of organic carbon are trapped in frozen northern circumpolar permafrost soils, which is about four times more than the total amount of carbon released by modern human activities and twice as much as is present in the current atmosphere (Tarnocai et al., 2009; Schuur and Abbott, 2011). The warming induced permafrost degradation is expected to drive changes in climate forcing, partially due to increasing microbial decomposition of soil organic carbon, which could release a large amount of soil carbon back into the atmosphere as CO_2 and CH_4 (Zimov et al., 2006; Schuur et al., 2009). The release of greenhouse gases may in turn accelerate global warming (Lashof and Ahuja, 1990). Understanding the impacts of permafrost thaw on microbially induced organic carbon degradation is critical to understanding feedbacks between terrestrial ecosystems and climate change.

A critical component of understanding organic carbon degradation is the quantification of physiochemical–biological processes that occur during freeze–thaw transitions. A large body of literature has explored how freeze–thaw processes impact microbial functioning across scales, from studying the plasma membrane of cells (Steponkus and Lynch, 1989) to feedbacks between microbial biogeochemical transitions and regional and landscape processes (Callaghan et al., 2004). Watanabe and Ito (2008) and Panikov (2009) showed that microbial activity is strongly dependent on the temperature and unfrozen water content, and microbial activity was found to decrease exponentially with decreasing temperature in the 0°C regime. Thawing of frozen soil increases nutrient availability to microbes, for example, through enhanced diffusion through disrupted soil aggregates (Sharma et

al., 2006) or through generating new nutrients from lysed soil microbes (Morley et al., 1983). The freeze–thaw process of ice-rich soil is directly related to cryoturbation and redistribution of organic carbon in permafrost (Bockheim, 2007, and reference therein), greatly affecting its vulnerability for degradation and hydraulic pathways needed for nutrient and moisture delivery.

Freeze–thaw transitions vary significantly over space and time (Zhang et al., 2004; Han et al., 2010). Quantification of spatiotemporal freeze–thaw dynamics is important for improved prediction of their effects on climate change. Although multiple methods, including geological map and aerial photograph examination, direct wellbore measurements, and geophysical and remote sensing methods, have been used for permafrost mapping (Ferrians and Hobson, 1973; Hoekstra et al., 1974; Hilbich et al., 2008; Kneisel et al., 2008), methods to monitor permafrost freeze–thaw transitions are limited. Other than direct temperature measurements through point ground sources, such as ground and wellbore based temperature sensors, satellite based radar and radiometer measurements have been proposed and tested and can provide snapshots of the freeze–thaw state of the ground surface at large (regional and global) scales with resolution from a few to tens of kilometers (Running et al., 1999; Entekhabi et al., 2004; Kimball et al., 2004). While wellbore measurements provide direct but sparse point data and satellite based remote sensing methods provide much larger spatial coverage but with limited resolution, surface based geophysical methods offer an avenue to improve the quantification of freeze–thaw transitions in high resolution and over landscape scales. Although time-lapse surface geophysical methods provide spatially extensive information about subsurface variability and dynamics in a noninvasive manner, quantitative interpretation of geophysical data in terms of hydrological, biogeochemical, or geomechanical properties requires an understanding of the petrophysical relationships that link the geophysical attributes (e.g., electrical resistivity or seismic velocity) with freeze–thaw characteristics (e.g., soil moisture content, ice content, or temperature).

The most frequently used geophysical methods for permafrost or frozen soil studies include electrical methods (resistivity and induced polarization [IP]), ground penetrating radar, and seismic refraction (Fortier et al., 1994, 2008; Fortier and Allard, 1998; Kneisel et al., 2008, and references therein; Vanhala et al., 2009). In this study, we explored the potential of the complex resistivity method for monitoring of freeze–thaw transitions in the arctic soil at the laboratory scale. Our objective was to gain an understanding of the sensitivity of complex resistivity responses to the freeze–thaw transition as a foundation for exploring the utility of the method for monitoring spatiotemporal variations in freeze–thaw transitions over field-relevant scales. This was achieved through laboratory column experiments designed to simulate temperature induced freeze–thaw transitions with concurrent temperature and complex resistivity measurements. Interpretation of the complex resistivity data was focused on the evaluation of the sensitivity of

the complex resistivity measurements to the characteristics of the different stages of freeze–thaw transitions defined on the basis of temperature measurements.

◆ Electrical Methods And Applications In Permafrost Studies

Electrical methods study charge conduction properties of the target material. Measurements can be expressed as impedance (z), resistivity (ρ), conductivity (σ), or permittivity (ϵ); all are calculable from the impedance and sample geometry. Herein, we will use resistivity (or its reciprocal, conductivity) as these terms are commonly used in permafrost and electrical geophysical literature.

The electrical impedance of most soils is a complex term that exhibits frequency dependent behavior. Complex electrical signals, such as complex conductivity, σ^* , can be expressed in terms of a magnitude ($|\sigma|$) and a phase shift (ϕ) or a real (σ') and an imaginary (also called quadrature, σ'') component:

$$\sigma^* = \frac{1}{\rho^*} = i\omega\epsilon^* = \sigma'(\omega) + i\sigma''(\omega) \quad [1]$$

$$|\sigma^*| = \frac{1}{|\rho^*|} = \sqrt{\sigma'^2 + \sigma''^2} = \frac{1}{\sqrt{\rho'^2 + \rho''^2}} \quad [2]$$

$$\phi = \tan^{-1}\left(\frac{\sigma''}{\sigma'}\right) = -\tan^{-1}\left(\frac{\rho''}{\rho'}\right) \approx \frac{\sigma''}{\sigma'} \quad [3]$$

where ρ^* is the complex resistivity, ρ' is the real resistivity, ρ'' is the imaginary resistivity, ϵ^* is the permittivity, ω is the angular frequency, and $i = \sqrt{-1}$.

In terms of complex conductivity, the conductivity magnitude is a measure of the ability of the sample to conduct charges, and the phase shift or imaginary conductivity is a measure of the magnitude of polarization that predominantly occurs at mineral grain–electrolyte interfaces at low frequencies (Revil, 2012).

For a geological porous media, the magnitude and phase response (or real and imaginary components) of the complex term is a function of several properties. In particular, the magnitude of electrical conductivity is primarily determined by charge conduction through interconnected pore spaces (Archie, 1942). As such, soil characteristics such as porosity, permeability, temperature, saturation, and the salinity of the pore solution are all parameters that can affect conductivity signals. Charge polarization at low frequency is a surface phenomenon that is directly related to the charge redistribution and relaxation in the electrical double layer (EDL) structure at mineral–water interfaces that occur on the excitation by an external potential field. This charge polarization

is mainly an electrochemical phenomenon at low frequencies, and its magnitude is primarily controlled by EDL properties, such as its thickness, charge density, and mobility (Lesmes and Morgan, 2001). Additionally, the magnitude of charge polarization is affected by the amount of available mineral–water interfaces in the sample, which are in turn influenced by parameters such as saturation level, mineralogy, and size distributions.

Macroscopic models, such as the Cole–Cole type model (Pelton et al., 1978), can be used to fit the spectral electrical data to computer simple parameters that are frequency independent. Such parameters can be used to represent the global electrical property of the target samples, for example, resistivity and polarization magnitude. Using the Cole–Cole model, the frequency dependence of σ^* can be modeled as described by (Jones, 2002)

$$\sigma^*(\omega) = \sigma_0 \left\{ 1 + m \left[\frac{(i\omega\tau)^c}{1 + (i\omega\tau)^c (1 - m)} \right] \right\} \quad [4]$$

where σ_0 is the conductivity at direct current (DC) frequency, τ is the mean relaxation time, representing a polarization length scale (Scott and Baker, 2003; Revil and Florsch, 2010; Revil et al., 2012), c is a shape exponent (typically 0.1–0.6) related to the particle size distribution, and m is the chargeability and is a measure of the polarization magnitude.

For most natural soils that contain little or no metallic minerals, their polarization anomalies are normally small (in the range of a few to tens of milliradians in terms of phase response). Because the polarization magnitude of natural soils is directly related to the amount of available surface area per unit sample (or pore) volume, polarization measurements can be used to estimate specific surface area or clay content in soils (Schön, 1996; Slater et al., 2006; Weller et al., 2010). Temperature can also affect polarization signatures and has been observed in recent studies (Tong and Tao, 2007; Zisser and Kemna, 2010). Temperature can affect polarization through altering ionic activity and charge mobility (Murrmann, 1973) as well as impacting the thickness of the EDL (Grahame, 1947). Effects of these aforementioned parameters on charge polarization signals were studied mostly for unfrozen samples. However, in the case of permafrost studies, the freeze–thaw process and associated transition of water between liquid and ice are expected to play the dominant role in controlling charge polarization signals (as will be discussed below).

Electrical methods have been used for a wide variety of Earth science applications, from early mineral explorations (Bertin and Loeb, 1976; Sumner, 1976) to recent hydrological and biogeochemical studies in the near surface (Rubin and Hubbard, 2005; Slater, 2007; Atekwana and Slater, 2009; Williams et al., 2009). The most widely used approach—electrical resistivity tomography (ERT)—measures resistivity magnitude through injection of DC

current into the subsurface. Resistivity survey provides information on the electrical resistivity structure of the subsurface, which can be used to infer, for example, lithological or hydrological information (Lesmes and Morgan, 2001; Binley and Kemna, 2005; Lesmes and Friedman, 2005). With an IP survey, both resistivity and polarization signals are measured in the time or frequency domain. In the time domain, the polarization magnitude is evaluated through inspecting the decay curve of the potential field after the external current has been shut off. In the frequency domain, the potential waveforms measured on the samples are compared with those from a precision reference resistor to infer a magnitude difference and a phase shift value. Traditional frequency domain IP survey is normally conducted at a single or a few discrete frequencies. Recently, spectral induced polarization or complex resistivity methods have been increasingly used for characterization of the shallow subsurface. This method measures the complex electrical behavior of the material under study over a spectrum of frequencies (e.g., from 0.1 to >1000 Hz). Several recent studies have demonstrated how complex resistivity based information about the relaxation time scale of the surface charge polarization can be useful for hydrological as well as biogeochemical investigations (Slater, 2007; Atekwana and Slater, 2009).

Electrical methods are very useful for characterizing frozen soil environments because the contrast of resistivity between frozen and unfrozen soils is very large (often times a few orders of magnitude). Depending on temperature, ice content, and soil type, typical permafrost soils have resistivity values ranging from tens to hundreds of kilo ohm meters ($k\Omega\ m$) (French et al., 2006; Krautblatter and Hauck, 2007; Fortier et al., 2008). In contrast, the resistivity of unfrozen soil normally ranges from a few thousand down to tens of ohm meters ($\Omega\ m$), again depending on factors such as temperature, moisture content, pore water salinity, and soil type and texture. Temperature has a major effect on electrical resistivity. While linear correlation between temperature and electrical resistivity at above 0°C is well established (Hayley et al., 2007; Krautblatter and Zisser, 2012), at below 0°C both linear and exponential correlations between temperature and electrical resistivity have been observed for various samples (McGinnis et al., 1973; Krautblatter and Zisser, 2012). It has been postulated that while exponential correlation might be applicable to loose and highly permeable materials, a linear correlation exists for low permeability rocks with isolated water saturated pores (Krautblatter and Zisser, 2012).

In permafrost environments IP surveys were explored in earlier years (Sidorova and Fridrikhsberg, 1973; Olhoeft, 1977), but more recently ERT has become the dominantly used method (Fortier et al., 2008; Kneisel et al., 2008; Vanhala et al., 2009; Krautblatter et al., 2010). This recent preference could be due to the improved ease in collecting multiplexed ERT data, the relatively larger noise level of the IP data due to electromagnetic coupling effects from the measurement cables when alternating current is injected, and the difficulty in interpreting the IP data due to the variety of mechanisms that influence the signal. Electrical methods have

been used for a variety of different types of frozen system investigations. Electrical resistivity methods have been successfully used to delineate regions having different quantities and types of ground ice (Yoshikawa et al., 2006; DePascale et al., 2008; Hauck et al., 2010) and to detect and map permafrost (Fortier and Allard, 1998; Mühl et al., 2002; Kneisel et al., 2008; Vanhala et al., 2009). Some studies have also used electrical resistivity to understand permafrost dynamics over time (Krautblatter and Hauck, 2007; Hilbich et al., 2008). Krautblatter and Hauck (2007) studied electrical resistivity variation within 1 or 2 mo in permafrost of solid rock walls associated with warming or cooling. Hilbich et al. (2008) studied resistivity variation of mountain permafrost over a 7-yr period and identified changes over seasonal, annual, and long-term scales.

Several of these studies indicate that resistivity alone can be satisfactorily used to separate frozen from unfrozen soils with acceptable uncertainty. However, its ability to provide high resolution information at the freeze–thaw transition in circumzero regimes is limited. This is partially because temperature is only one of the major factors controlling electrical resistivity, and it is often difficult to separate temperature effects from those exclusively related to the freeze–thaw process itself. For example, when a frozen sample is brought into an environment above 0°C, there is an initial decrease of resistivity partially due to temperature increase before the sample starts to thaw (Hoekstra et al., 1974; Delaney et al., 2001). Slight pore ice thaw can also occur as a sample approaches 0°C from subzero temperatures (Penner, 1970) and contribute to resistivity decreases. At close to 0°C, the thawing process starts and the sample enters an isothermal stage where temperature stays constant. This isothermal point could be at 0°C or slightly below 0°C depending on the severity of freezing point depression (Low et al., 1968; Anderson and Tice, 1972; Banin and Anderson, 1974; Hall et al., 1988). Increased salinity enhances freezing point depression, and during a gradual freezing process a pore water salinity gradient can be set up due to progressive ion exclusion (Anderson and Morgenstern, 1973; Stahli and Stadler, 1997), thus leading to potential differences in isothermal points at different locations of the samples.

During the thawing process, the electrical resistivity is expected to continue to decrease due to the dramatically increased volume fraction of unfrozen water as well as mobility of water and solute molecules or ions, enhancing electrical conductivity.

Because of the critical importance of the freeze–thaw transition on permafrost hydrology, microbial activity, and their associated impacts on carbon dynamics, the ability to reliably detect the onset and dynamics of this transition is desired. Resistivity changes could be useful to study the freeze–thaw transition; however, its capability is limited. We posit that the much less explored IP, and especially complex resistivity, method could provide significant insights about the spatiotemporal distribution of this critical transition because of the fundamental linkage between the polarization signals and the state of the pore water (i.e., frozen vs. unfrozen). Theoretically,

at low frequencies a completely frozen soil could not generate an electrochemical polarization signal at the mineral–water interface because most of the water and solute molecules and ions are “locked up” in the ice matrix; therefore, their ability to polarize at the mineral–water interface is greatly restricted. Note that dielectric relaxation of ices (pure or with saline or mineral impurities) have been studied and charge polarization and relaxation of the ice were related to orientational Bjerrum defects or Maxwell–Wegner effects at high frequencies (Bjerrum, 1952; Gränicher et al., 1957; Gruen and Marcelja, 1983; von Hippel, 1988; Grimm et al., 2008; Stillman et al., 2010). Unlike electrochemical polarization that relies on the diffusion of the charged ions along the mineral–water interfaces, ice polarization related to Bjerrum defects and Maxwell–Wegner effects are caused by water molecule rotation under external potential fields or conductivity contrast between two discontinuous layers (Stillman et al., 2010). For electrochemical polarization at low frequencies, the capability of the ions to move along the mineral surface is the premise; therefore, no polarization signal from the mineral–water interfaces can be generated if the pore water is frozen. Once thawing starts and a portion of the previously “locked-up” ions become mobile, a polarization effect is expected to become evident. The magnitude of the polarization should increase as thawing progresses and the fraction of liquid water increases and reach a maximum on complete thaw of the sample. During this freeze–thaw transition, isothermal condition prevails, thus the temperature effects on polarization signal can be neglected. However, if temperature continues to rise above zero, additional changes of polarization signal may be observed on the basis of previous discussion on the effect of temperature on EDL properties. During freeze–thaw transition, the magnitude of the polarization response is dependent on the amount of thawed versus frozen water in the soil. As such, the polarization response could be used to quantify the relative fractionation between unfrozen and frozen water during this transition. This could be very useful as unfrozen water content is one of the major factors impacting microbial functioning as discussed above.

It is important to note that a small fraction of liquid water still exists even at temperature below –10°C (Watanabe and Mizoguchi, 2002; Wang et al., 2006). This liquid water likely exists as isolated water “pockets” in an otherwise frozen soil matrix. A continuous temperature decrease below –10°C has a relatively smaller impact on liquid water content when compared with temperature at ~0°C. Such small changes of water content might not have major impacts on resistivity when compared to the effect of temperature change itself. In addition, such isolated water pockets are unlikely to produce readily observable electrochemical polarization signals because of their limited volume fraction and, more importantly, spatial discontinuity. In addition, at such temperatures electrodes for polarization measurements are normally surrounded by frozen soil or ice, which can dramatically increase the contact resistance and results in difficulty getting reliable polarization signals.

We posit that more detailed information about the freeze–thaw transitions are potentially obtainable using time-lapse complex resistivity data. For instance, soil texture influences freeze–thaw behavior; clay-rich soils tend to freeze later and thaw earlier relative to sand-rich soils because they have a lower freezing point due to their small pore radii and high capillary potentials (Everett, 1961; Blachere and Young, 1972). Because the frequency response of the complex resistivity spectrum is related to the distribution of a polarization length scale, being a characteristic pore dimension or size distribution of the polarizable particles (Wong, 1979; Olhoeft, 1985; Dias, 2000; Scott and Baker, 2003; Revil and Florsch, 2010; Revil et al., 2012), and in this study only the thawed portion of the bulk material is presumably polarizable during freeze–thaw transition, we further hypothesize that we can use the spectral data to document freeze–thaw behaviors as a function of soil texture variability.

Materials and Methods

Materials

The soil samples used for the laboratory studies were collected from BEO. Barrow (71.3°N, 156.5°W) and the BEO lie within the Alaskan Arctic Coastal Plain, a relatively flat region bordered on the north by the Arctic Ocean and on the south by the foothills of the North Slope. Permafrost at the site is continuous, ice rich, and present to depths greater than 350 m (Sellmann, 1975). The active layer thickness is small, varies with topographic position, and averages 30 to 35 cm (Shiklomanov et al., 2010). The mean annual air temperature is -11.3°C , and the mean annual precipitation is 106 mm with the majority falling as rain during the short summer. Soils are classified as Gelisols and are characterized by an organic-rich surface layer underlain by a horizon of silty clay to silt loam textured mineral material and a frozen organic-rich mineral layer.

Soil samples were collected using a Russian corer (Aquatic Research Instruments) from the active layer during the end of the growing season (September 2011). Cores were 5 cm in diameter and typically a few centimeters to ~ 28 cm in length (Hubbard et al., 2012). The average depth to the permafrost near the sample acquisition site is 36 cm. Multiple samples were collected across a geomorphologic gradient (from high to low centered polygons). Texture analysis of 18 samples collected across this transect indicated that the mineral soil texture is predominantly a sandy clay loam with ~ 20 to 30% clay, ~ 20 to 30% silt, and ~ 40 to 60% sand. Because of the small sample size collected at each location and the similarity in the texture of the individual samples, samples were combined for the column experiments. The gravimetric moisture content of the combined sample was $\sim 65\%$, and the organic matter was $\sim 26\%$ based on loss on ignition measurements. The fluid conductivity of the extracted pore water was $\sim 300 \mu\text{S}/\text{cm}$. The samples were kept frozen at -20°C until the start of the experiments. The soil samples were combined and mixed with a spatula before being packed into the columns. Because the soils were moist and clumpy and difficult to mix homogeneously, the combined samples were expected to be reasonably heterogeneous.

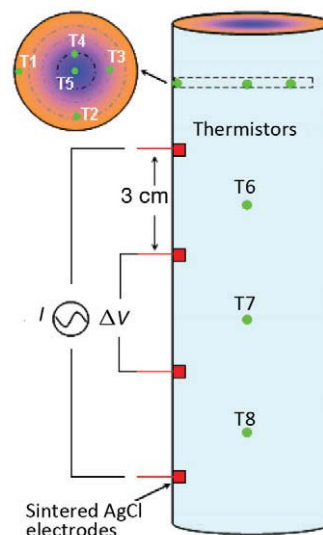


Fig. 1. Schematic design of the column for the experiments. The red squares are locations of sintered AgCl electrodes, and the green dots are location of the thermistors (T) used for temperature measurements.

Column Design and Soil Packing

The column used for the experiments was constructed with transparent schedule 40 PVC tube with a 5.08 cm diameter and a length of 12 cm. Ports for electrodes and temperature sensors were drilled on the column wall; a schematic configuration of the column is shown in Fig. 1.

The electrodes used for complex resistivity data acquisition were Ag/AgCl electrodes (In Vivo Metric) with a sintered AgCl stub (~ 2 mm long) attached to a lead Ag wire. The electrodes were embedded into the column to enable direct contact with the soil samples for enhanced electrical connectivity. Four electrodes were installed with the outer two used for current injection and the inner two used for potential measurements (Fig. 1). The interval between a pair of adjacent electrodes was 3 cm.

Eight thermistors (T type, 0.1% accuracy, Newark Electronics) were also buried into the soil during column packing for real-time temperature monitoring using an Agilent LXI datalogger (Agilent). The thermistors were made of thermal sensitive resistors, and the temperature values were calculated from resistance values based on predetermined calibration curves between resistance and temperature. The geometric arrangement of the thermistors is shown in Fig. 1. The choice about the number and location of the thermistors was made to balance sensor density with structural and thermal interruption from the sensors. Five of the eight thermistors (T1–T5) were installed along a single horizontal cross section of the column at different distances into the soil from the column wall. These thermistors were distributed along this core plane to minimize interruption to soil structure as well as to thermal conduction patterns. The other three thermistors (T6–T8)

were installed in the center of the column and spaced evenly with respect to their depths into the column in the vertical direction (Fig. 1) for evaluation of the uniformity of temperature change across the entire column. The wires for the thermistors were insulated with plastic sleeves to minimize their impacts on thermal and electrical properties of the soil.

The mixed soils were packed into the column at ~ 1 cm per step using a spatula, and the introduced soils were compressed with a plastic rod matching the inner diameter of the column after each step to minimize size and volume of void spaces and to enhance homogeneity and ensure connectivity with the electrical and temperature sensors. The temperature sensors were inserted into the column during the packing process. A 2-cm gap was left on top of the column to accommodate frost heave. This packing method may lead to hydraulic properties that are not representative of site conditions. To preserve in situ hydraulic properties, intact cores should be used but were not available during these experiments. For the purpose of this experiment, the mixed and repacked samples were deemed to be acceptable.

Once packed, the column was placed into a -20°C freezer for setting up the initial frozen condition. The lead wires for electrical and temperature measurements were routed to the instrumentations outside of the freezers.

Electrical Measurements

Electrical measurements were collected with a National Instruments dynamic signal analyzer (DSA, NI4461) using the electrodes placed along the length of the column (Fig. 1). A pre-amplifier was used to boost the input impedance to $10^9 \Omega$ to minimize current leakage into the measurement circuitry. Water column tests were conducted to evaluate repeatability and noise level of the system. For this, the column was filled with electrolyte having similar conductivity ($\sim 100 \mu\text{S}/\text{cm}$) of the soil samples (Hubbard et al., 2012), and electrical signals were measured. These tests indicate that errors were less than 2 mrad for the phase and 0.5% for resistivity at low frequencies (< 1000 Hz), indicating high data quality. Each measurement was composed of a phase shift (ϕ) and a magnitude ($|\sigma|$) component recorded relative to a precision reference resistor for 40 frequencies spaced at equal logarithmic intervals from 0.1 to 1000 Hz. The real and imaginary parts of the complex conductivity represent the magnitude of the conduction and polarization of the sample, respectively, and can be calculated using the following equations:

$$\sigma' = |\sigma| \cos \phi \quad [5]$$

$$\sigma'' = |\sigma| \sin \phi \quad [6]$$

Selected datasets were inverted for Cole–Cole parameters (Eq. [4]) using an algorithm based on a least-squares approach with Marquardt regularization (Kemna, 2000).

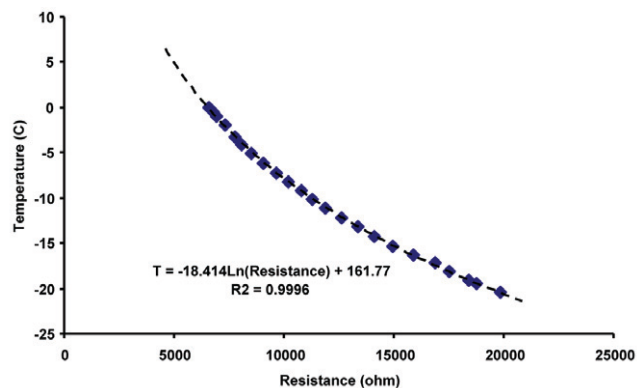


Fig. 2. Resistance and temperature correlation curve for Thermistor T1.

Experimental Procedure

After being kept in the -20°C freezer for at least 24 h to ensure initial frozen status and thermal equilibration, the column was quickly switched into a 4°C refrigerator for ~ 30 h to induce thawing. After complete thaw and thermal equilibration at 4°C , the column was then switched back to -20°C again to induce freezing. After ~ 20 h at -20°C , the column was transferred back to 4°C and then back to -20°C again following the same procedure in the first cycle. These two repeated cycles were primarily aimed to evaluate repeatability of the measurements. During these freeze–thaw transitions, both complex resistivity and temperature measurements were logged on a regular basis. The calibration curves for the thermistors were developed in the temperature range -20°C and used for temperature calculation.

Results and Discussion

Interpretation of the correlation between freeze–thaw transition and electrical responses relies on accurate temperature measurements that were used to define the different stages of the process. The eight thermistors used in the experiment were calibrated over a temperature range from 0 to -20°C ; as an example, the calibration curve for Thermistor T1 is shown in Fig. 2. A natural log correlation ($R^2 > 0.99$ for all thermistors) between thermistor resistance and temperature was developed for all eight sensors.

Experimental Repeatability

Figure 3 shows an example of changes in electrical resistivity and temperature at locations T5 and T7 during the two freeze–thaw cycles, revealing excellent repeatability. Note that temperature fluctuations, most noticeably between 2000 to 3000 min and those at > 5000 min, were caused by the power cycle of the -20°C freezer used in the experiments. Similar fluctuations with smaller magnitude were observed between 1000 to 2000 min and 4000 to 5000 min for the similar reason in the 4°C refrigerator. These temperature fluctuations caused variations in resistivity due to the influence of temperature on electrical resistivity discussed above. Because of

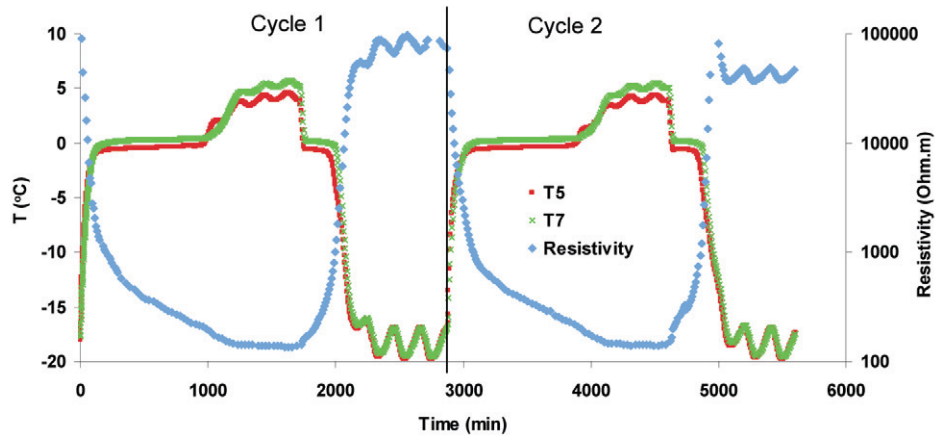


Fig. 3. Changes of electrical resistivity and temperatures at T5 and T7 during the two freeze–thaw cycles, demonstrating repeatability of the measurements.

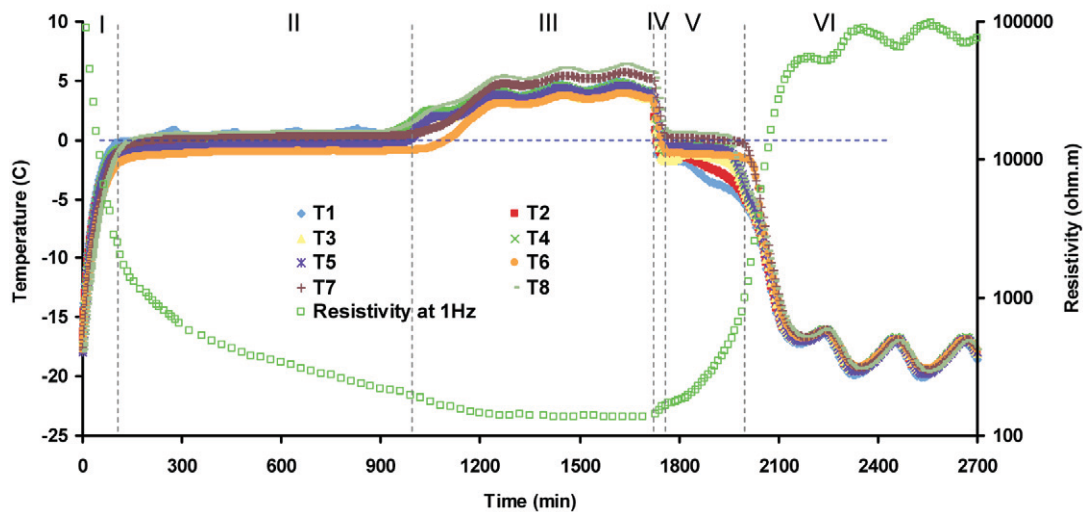


Fig. 4. Changes of temperature and electrical resistivity at 1 Hz during freeze–thaw transition. The freeze–thaw cycle is divided into six stages: Stage I, initial temperature increase at below 0°C; Stage II, isothermal thawing; Stage III, temperature increase above 0°C; Stage IV, temperature decrease at above 0°C; Stage V, isothermal freezing; and Stage VI, temperature decrease at below 0°C.

the excellent repeatability between these two freeze–thaw cycles, the following discussion will focus only on the first cycle.

It is also worthy to note that freeze–thaw transitions in these column experiments generally progressed from the wall of the column to the center and were expected to be symmetrical in the radial dimension. This is different from the actual in situ freeze–thaw transitions in arctic environments where primarily one-dimensional vertical progression from ground surface to depth is expected. However, the current column design suffices for the objectives of this study.

Resistivity Changes During Freeze–Thaw Transition

Changes of electrical resistivity of the column as well as temperatures at the eight thermistor locations during freeze–thaw transition are shown in Fig. 4.

On the basis of the characteristic temperature changes, the freeze–thaw cycle during the experiment can be divided into the following six stages: Stage I, initial increase of temperature before thawing starts at ~0°C; Stage II, isothermal thawing of the soil column at ~0°C; Stage III, temperature increase and fluctuation at above 0°C following complete thawing of the sample; Stage IV, initial decrease of temperature before freezing starts; Stage V, isothermal freezing of the soil sample at ~0°C; and Stage VI, continued temperature

decrease following freezing of the sample. We will use these six stages as references for the following discussions. Note that from Stages I to III, the sample was kept at 4°C, and from Stages IV to VI, the sample was kept at -20°C. When comparing the time scale between the isothermal thawing (Stage II) with freezing (Stage V) stages, one could notice that the time requirement for the column to thaw is much longer than that for it to freeze. This is because the temperature gradient between the isothermal point (~0°C) and the ambient during the thawing process (4°C) is much smaller than that during the freezing process (20°C), causing different levels of thermal forcing during these two periods.

Examination of the temperature profiles from T1 to T8, specifically during the thawing (Stage II) and freezing (Stage V) periods, yields useful information with respect to the freeze-thaw characteristics of the column (Fig. 4). First to notice is the difference in isothermal points, roughly ranging from 0 to -1°C, at these different locations during Stages II and V. The data suggest a pattern where the sensors located closer to the column wall (especially T1) showed higher isothermal points than those at the inner column locations. Our experiments suggested that freezing (and thawing) started from the wall and progressed to the center of the column; therefore, a pore water salinity gradient from the wall to the center could have been set up during freezing due to progressive ion exclusion as discussed above, thus leading to the different levels of freezing point depression and different isothermal points.

Resistivity changes at various magnitudes were observed during the different stages of the freeze-thaw transition as indicated in Fig. 4. An initial resistivity decrease of nearly two orders of magnitude from ~100 kΩ m to a few thousand ohmmeters was observed when the temperature of the frozen sample was raised from -20 to ~0°C in Stage I. As discussed above, this initial decrease of resistivity is primarily related to temperature increase with some contributions from the increase of a small percentage of unfrozen water in the frozen soil matrix. During the isothermal thawing process in Stage

II where temperature stayed constant at ~0°C, a further decrease of resistivity was observed, which is interpreted to be primarily due to the thawing of the soil and mobilization of the pore fluid, enhancing its electrical conductivity. The resistivity of the soil decreased from ~2000 to ~200 Ω m, an order of magnitude decrease during the thawing process in Stage II. Resistivity was observed to continue to decrease slightly during Stage III, which is directly related to the increase of temperature of the completely thawed column from 0°C to the ambient temperature at ~4°C. When the thawed column was switched back into the -20°C freezer, an increase of resistivity was observed in Stage IV, which is interpreted to be solely due to the temperature decrease of the column before freezing occurred. This period was short in time due to the large temperature contrast between the column and the ambient environment within the freezer. Following Stage IV, where a moderate increase in resistivity was observed, a continuous increase of resistivity (from <200 to ~700 Ω m) was observed during column freezing in Stage V. This is the reverse of what was observed in Stage II and is interpreted to be primarily related to the transition of the soil from unfrozen to frozen, significantly reducing its electrical conduction capability. Continued increase of resistivity over two orders of magnitude was observed during Stage VI, which is interpreted to be associated with the temperature decrease of the frozen soil until it reached the ambient level and started to fluctuate with the temperature fluctuation cycle within the -20°C freezer.

The experimental data suggest temperature is one of the dominant factors controlling electrical resistivity throughout the freeze-thaw transition. Correlations between temperature and resistivity during the frozen and unfrozen stages are plotted in Fig. 5. The temperature values in Fig. 5 are averaged from the eight temperature sensors embedded in the column with standard deviation plotted as error bars.

Figure 5 shows that different types of correlations between temperature and electrical resistivity were observed depending on the stages during the freeze-thaw transition: an exponential

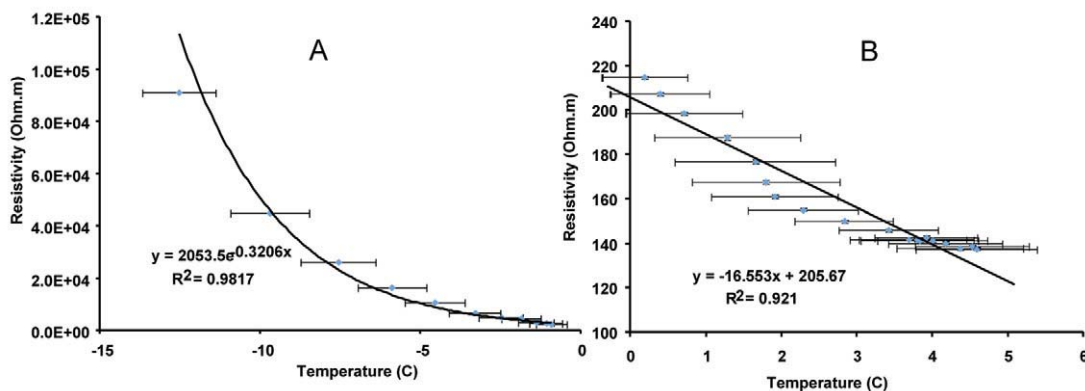


Fig. 5. Correlation between electrical resistivity and soil temperature at temperature (a) below 0°C and (b) above 0°C. The error bars represent standard deviations of the average temperature from all eight temperature sensors.

correlation was observed for frozen soils (Fig. 5a), and a linear correlation between resistivity and temperature exists for unfrozen soil (Fig. 5b). While the linear correlation between temperature and electrical resistivity at above 0°C is consistent with previous studies as discussed above, our observation of an exponential correlation between temperature and resistivity at temperature at below 0°C supports the observations of McGinnis et al. (1973). Krautblatter and Zisser (2012) observed a linear correlation between temperature and resistivity for water saturated, low permeability permafrost rocks from high mountains and hypothesized that the different types of correlations were related to the different particle packing and permeability structure of the samples. Our soil samples were loosely similar to the samples tested by McGinnis et al. (1973) and are consistent with this hypothesis.

Overall, significant changes in electrical resistivity were observed during the freeze–thaw transition, and the large resistivity contrast between frozen and unfrozen soil allows them to be distinguished based solely on resistivity with a priori knowledge of the resistivity ranges for the frozen and unfrozen soils. However, detailed information about the different stages or freeze–thaw transitions is difficult to extract from the resistivity data without the assistance of other data types (in this case temperature data), specifically during the isothermal phase transition between ice and water (Stages II and V of our experiment).

Polarization Response During Freeze–Thaw Transition

Figure 6 shows the changes of the electrical phase response and imaginary conductivity at 1 Hz during the freeze–thaw transition. A distinctive pattern for electrical phase signals—much different from that of the resistivity—was observed. Meaningful phase

signals were only recorded during Stages II, III, IV, and the beginning part of Stage V. This observation is largely consistent with previous assumptions that no low frequency electrochemical polarization signals can be observed for frozen soils (Stages I and VI of the experiment). Stage V is an exception and will be discussed below.

Figure 6 show that no phase signal was observed until the beginning of Stage II (when the column started to thaw). The phase response subsequently increased continuously with the progression of thawing (i.e., increasing amount of liquid water in the soil matrix) and reached a maximum value at the end of Stage II when the soil was completely thawed. This is consistent with our hypothesis that at low frequency the electrical phase response is exclusively associated with liquid water because phase responses are associated with the EDL near mineral–water interfaces, which only exhibit polarization behavior when the pore water is unfrozen. During the thawing process of the soil, the increase of the unfrozen water content increases the amount of surface area with viable surface charge and, therefore, increases the polarization signal. Such a correlation indicates that the electrical phase response can be potentially used as an exclusive proxy for the monitoring of the onset and progression of the thawing process of frozen soils. Furthermore, estimation of the fractionation between unfrozen and frozen soil can be performed on the basis of the magnitude of the phase signal. Note that parameters such as pore fluid saturation, salinity, and temperature are factors that could impact the electrical phase response on the basis of the previous discussion. However, these parameters primarily affect the electrical signature when the pore water is unfrozen and are thus secondary compared to the effects of the freeze–thaw transition itself. Figure 6 also shows that the imaginary conductivity changes during Stage II were very similar

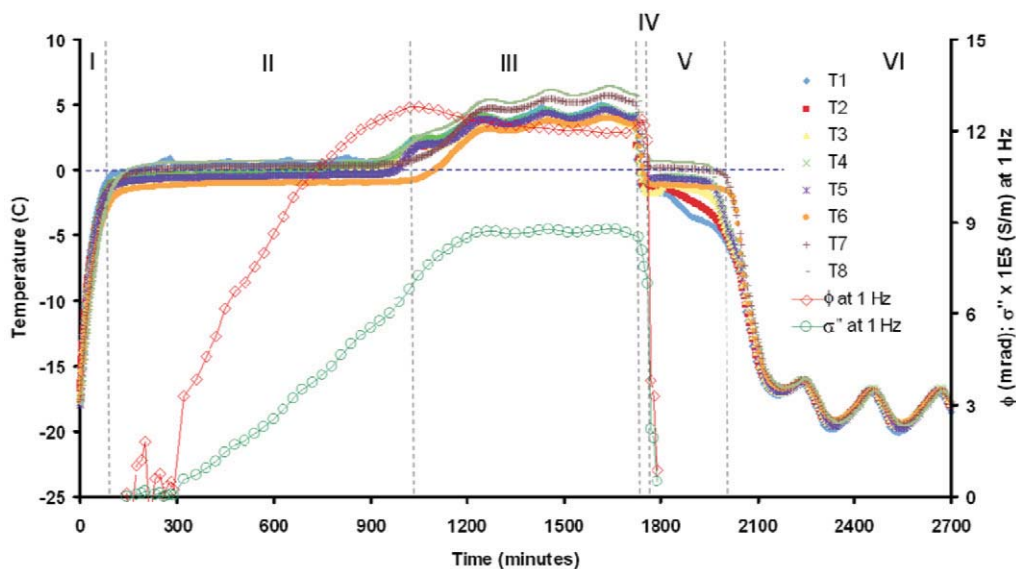


Fig. 6. Changes of temperature and electrical phase (ϕ) and imaginary conductivity (σ'') at 1 Hz during freeze–thaw transition. Note that imaginary conductivity values are multiplied by 105.

to that of the phase response and gradually increased with increasing amount of the thawed soil.

During Stage III (when the soil had completely thawed and the temperature continued to increase from 0 to 4°C), a small but gradual decrease of the phase response at 1 Hz was observed. We interpret this small decrease to be associated with the temperature increase. Because the phase is roughly the ratio between the imaginary and real components of the electrical signal (Eq. [3]), this decrease of the phase is primarily due to the more rapid increase of the real electrical conductivity of the column relative to the imaginary conductivity in responding to the temperature increase. Different from the phase response, Fig. 6 shows a short period of continued increase of the imaginary conductivity before it became stable for the duration of Stage III. Relative to imaginary conductivity, phase response seems to provide a better benchmark of the completion of isothermal thawing of the frozen soil in this study.

A quick decrease of the phase response at 1 Hz was observed during the temperature decrease followed by the soil freezing process in Stages IV and V, which is interpreted to be due to the transition of the pore water from unfrozen to frozen state. It is interesting to note that the phase signals were only recorded during the first few minutes of Stage V, which disappeared before completion of the freezing of the soil. We interpret this to be due to the inability of electrodes located near the column wall to record phase signals during freeze-up because of a large increase in contact resistance between the electrodes and the soil from ice formation. This effect is reversed during thawing processes in Stage II, in favor of phase data acquisition. The change of imaginary conductivity was very similar to the phase response during this period.

In general, single frequency phase response and imaginary conductivity at 1 Hz during the freeze–thaw transition demonstrated the potential of the polarization signals to provide precise information about the onset and progression of the freeze–thaw process. Given the ease of acquiring single, low frequency phase data at the field scales relative to spectral responses, we expect that this method should be able to provide useful information about spatiotemporal variations of freeze–thaw transitions in permafrost regions.

Spectral Electrical Response and Freeze–Thaw Characteristics

Figure 7 shows changes of spectral phase and imaginary conductivity responses during the thawing process in Stage II. This figure shows that in addition to the previously discussed increase of phase response and imaginary conductivity for those data points at 1 Hz, a clear shift of the spectral response is also observed during the thawing process of the soil in Stage II. This shift of the spectral response, manifested by the shift of the critical frequency with maximum phase values of each spectrum from ~30 to ~60 Hz (Fig. 7a), is interpreted to be caused by the increase of the charge relaxation time scale originated from an increase of average particle

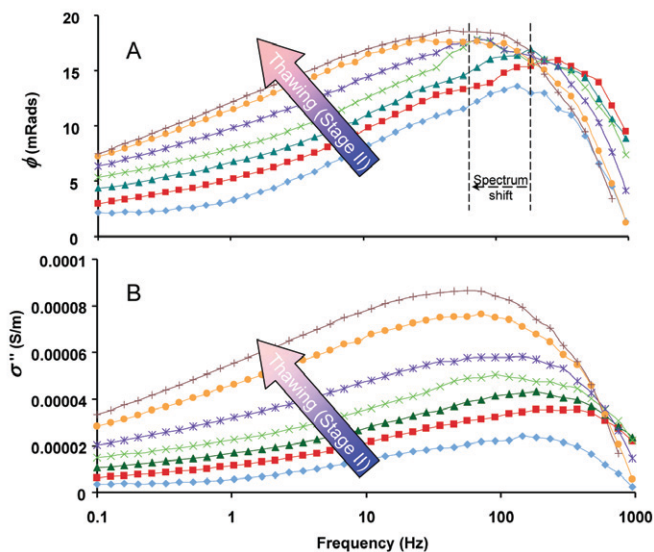


Fig. 7. Spectral electrical responses during the thawing process in Stage II (from 323 to 900 min of Fig. 6) of the experiment: (a) phase (ϕ) and (b) imaginary conductivity (σ'').

or a characteristic pore size of the thawed (i.e., polarizable) fraction of the bulk sample. This is related to the different thawing potential of particles having different grain sizes (i.e., clay-rich zones tend to thaw earlier compared to sand-rich zones), resulting in an increase of the average particle or pore size of the thawed portion of the soil during the progression of thawing. A reasonable amount of clay (~20–30%) was present in the soil samples used for the experiment and is potentially responsible for the initial phase response with peak frequency at higher values observed during the early thawing. This shift of the spectrum response suggests the potential utility of the spectral electrical responses to study soil textural controls on the freeze–thaw dynamics. Changes of spectral imaginary conductivity (Fig. 7b) are very similar to the phase and show both an increase of the overall magnitude and a shift of the spectrum to lower frequencies during the thawing process. Increase of the imaginary conductivity is a measure of the polarization magnitude at the grain surfaces and is directly related to the amount of the thawed particles within the soil matrix.

The reversed transition of the spectrum response—from low to high frequency with decreasing magnitude—was expected during the freezing process in Stage V. However, because of the short time frame of the freezing process in the experiment and the early freeze-up of the soil around the electrodes that prevented reliable phase measurement for a prolonged period of time during freezing, such transition was not captured during our study. Nevertheless, a quick decrease of the phase response at single frequency during the early stage of the freezing process was observed as shown in Fig. 6. Improvements of column and electrode design are needed to address this issue and help to understand the expected phase transition during the reversed freezing process of the soil.

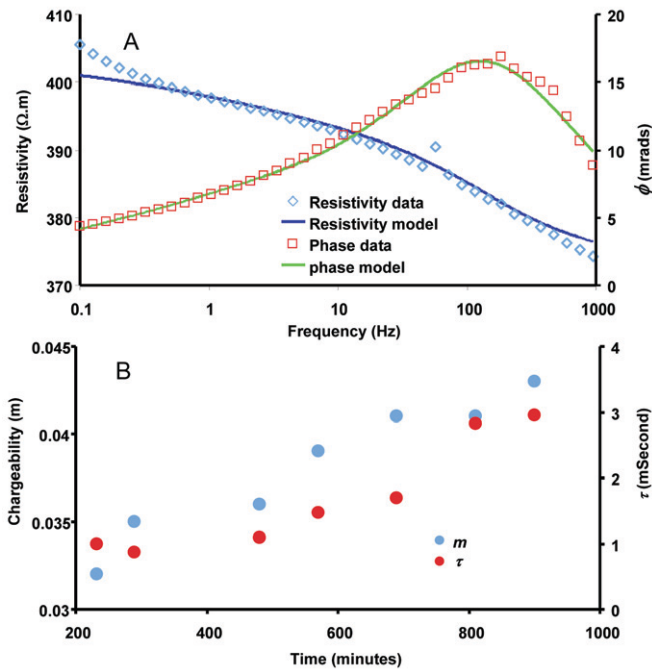


Fig. 8. (a) An example (data point at 480 min) of the Cole–Cole model fit to the spectral electrical data and (b) changes of chargeability (m) and time constant (τ) during isothermal thawing of the column during Stage II.

The Cole–Cole model was used to fit the spectral data shown in Fig. 7; an example of the model fit and change of chargeability (m) and time constant (τ) are shown in Fig. 8.

Figure 8 shows a continuous increase of both chargeability and time constant during the thawing process consistent with the increase of the phase and imaginary conductivity and the shift of the spectral response to low frequencies during thawing.

Summary and Conclusions

In this study, we conducted laboratory studies to explore the sensitivity of complex resistivity method to the freeze–thaw transition of soil samples collected for the arctic region. The column was instrumented with electrodes and thermistors for complex resistivity and temperature monitoring. Freeze–thaw transitions of the column were induced through shifting the sample between a 4°C refrigerator and a –20°C freezer. Electrical and temperature data were recorded regularly and automatically over two repeated cycles. Excellent repeatability was observed during the two cycles. On the basis of the experimental data, the following conclusions can be made:

1. Resistivity of the soil column varied over two orders of magnitude during temperature change between –20 and 0°C. Smaller resistivity variations were also observed during the

isothermal thawing or freezing processes. While resistivity changes in the former case are interpreted to be primarily related to temperature change, the latter is interpreted to be controlled by the fraction of unfrozen to frozen water during the freeze–thaw transition.

2. Single frequency phase responses and imaginary conductivity at 1 Hz were interpreted to be exclusively related to the presence of unfrozen water in the soil matrix and, therefore, can be used as a proxy for the monitoring of the onset and progression of the freeze–thaw transition. The magnitude of the phase response and imaginary conductivity is interpreted to be positively related to the amount of unfrozen water in the soil, which suggests that phase response and imaginary conductivity can potentially be used to quantify the fractionation between unfrozen and frozen water in the soil. Chargeability inverted from the Cole–Cole model increased during soil thawing, consistent with single frequency data.
3. The spectral electrical response contained additional information about the impacts of soil texture on freeze–thaw characteristics. Specifically, a shift of the spectral response to lower frequency was observed during the isothermal thawing process and is interpreted to be due to the sequential thawing from the fine to coarse particles within the soil matrix, thus increasing the average particle or pore size of the thawed (polarizable) fraction of the bulk material. Such changes were also observed with Cole–Cole parameters with the increase of time constant during thawing.

Our study has demonstrated for the first time the potential of complex resistivity for remote monitoring of the freeze–thaw transitions of the arctic soil, which is critical to the study of the geophysical, hydrologic, and biogeochemical transformations of the arctic region in a warming climate.

This study lays the foundation for utilization of the complex resistivity method at the field scale to monitor freeze–thaw transitions. Such monitoring is expected to provide insights about the spatiotemporal variability of controlling factors (moisture, texture). Importantly, such field monitoring should also be useful for constraining interpretation of biogeochemical data to quantify controls on and magnitude of greenhouse gas production during freeze–thaw transitions. In addition, results from this study also indicate opportunities for linking larger scale (millimeter to meters) electrical geophysical observations to pore scale processes and properties during freeze–thaw transitions. Specifically, the unique sensitivity of electrical polarization signals to interfacial properties and processes can be further explored to help improve our understanding of pore scale processes (e.g., fluid and ion migration and redistribution, mineralogical and biological transformations) during freeze–thaw transitions.

Acknowledgments

This research was conducted under the Next-Generation Ecosystem Experiments (NGEE Arctic) project supported by the Office of Biological and Environmental Research in the DOE Office of Science, through Contract No. DE-AC02-05CH11231 between Lawrence Berkeley National Laboratory and the U.S. Department of Energy" after "the DOE Office of Science. The authors thank the associate editor Mark Seyfried and two anonymous reviewers for constructive comments that helped to improve the manuscript.

References

- Anderson, D.M., and N.R. Morgenstern. 1973. Physics, chemistry and mechanics of frozen ground: A review. In: Permafrost: North American Contribution Second International Permafrost Conference, Yakutsk, Russia. 13–28 July 1973. Natl. Acad. of Sci., Washington, DC. p. 257–288.
- Anderson, D.M., and A.R. Tice. 1972. Predicting unfrozen water contents in frozen soils from surface area measurements. *Highw. Res. Rec.* 393:12–18.
- Archie, G.E. 1942. The electrical resistivity log as an aid in determining some reservoir characteristics. *Trans. Am. Inst. Min. Metall. Pet. Eng.* 146:54–62.
- Atekwana, E.A., and L. Slater. 2009. Biogeophysics: A new frontier in Earth science research. *Rev. Geophys.* 47:RG4004. doi:10.1029/2009RG000285
- Banin, A., and D.M. Anderson. 1974. Effects of salt concentration changes during freezing on the unfrozen water content of porous materials. *Water Resour. Res.* 10:124–128. doi:10.1029/WR010i001p00124
- Bertin, J., and J. Loeb. 1976. Experimental and theoretical aspects of induced polarization. Vol. I and II. Gebrüder Borntraeger, Berlin.
- Binley, A., and A. Kemna. 2005. DC resistivity and induced polarization methods. In: Y. Rubin and S. Hubbard, editors, *Hydrogeophysics*. Springer, Dordrecht, the Netherlands. p. 129–156.
- Bjerrum, N. 1952. Structure and properties of ice. *Science* 115:385–390. doi:10.1126/science.115.2989.385
- Blachere, J.R., and J.E. Young. 1972. The freezing point of water in porous glass. *J. Am. Ceram. Soc.* 55:306–308. doi:10.1111/j.1151-2916.1972.tb11291.x
- Bockheim, J.G. 2007. Importance of cryoturbation in redistributing organic carbon in permafrost-affected soils. *Soil Sci. Soc. Am. J.* 71:1335–1342. doi:10.2136/sssaj2006.0414N
- Callaghan, T.V., L.O. Björn, Y. Chernov, T. Chapin, T.R. Christensen, B. Huntley, R.A. Ims, M. Johansson, D. Jolly, S. Jonasson, N. Matveyeva, N. Panikov, W. Oechel, G. Shaver, S. Schaphoff, and S. Sitoh. 2004. Effects of changes in climate on landscape and regional processes, and feedbacks to the climate system. *Ambio* 33:459–468.
- Delaney, A.J., P.R. Peapples, and S.A. Arcone. 2001. Electrical resistivity of frozen and petroleum-contaminated fine-grained soil. *Cold Reg. Sci. Technol.* 32:107–119. doi:10.1016/S0165-232X(00)00023-9
- DePascale, G.P., W.H. Pollard, and K.K. Williams. 2008. Geophysical mapping of ground ice using a combination of capacitive coupled resistivity and ground penetrating radar, Northwest Territories, Canada. *J. Geophys. Res.* 113:F02S90. doi:10.1029/2006JF000585
- Dias, C. 2000. Developments in a model to describe low-frequency electrical polarization in rocks. *Geophysics* 65:437–451.
- Entekhabi, D., E.G. Njoku, P. Houser, M. Spencer, T. Doiron, Y. Kim, J. Smith, R. Girard, S. Belair, W. Crow, T.J. Jackson, Y.H. Kerr, J.S. Kimball, R. Koster, K.C. McDonald, P.E. O'Neill, T. Pultz, S.W. Running, J. Shi, E. Wood, and J. Vanzyl. 2004. The hydrosphere state (hydros) satellite mission: An Earth system pathfinder for global mapping of soil moisture and land freeze/thaw. *IEEE Trans. Geosci. Remote Sens.* 42:2184–2193. doi:10.1109/TGRS.2004.834631
- Everett, D.H. 1961. The thermodynamics of frost damage to porous solids. *Trans. Faraday Soc.* 57:1541–1551. doi:10.1039/tf9615701541
- Ferrians, O.J., Jr., and G.D. Hobson. 1973. Surveying and predicting permafrost in North America: A review, 1963–1973. In: Permafrost: North American Contribution Second International Permafrost Conference, Yakutsk, Russia. 13–28 July 1973. Natl. Acad. of Sci., Washington, DC. p. 479–498.
- Fortier, R., and M. Allard. 1998. Induced polarization and resistivity logging in permafrost. In: A.G. Lewkowicz and M. Allard, editors, *Proceedings of the Seventh International Permafrost Conference*, Yellowknife, Canada. 23–27 June 1998. Univ. Laval, Quebec, Canada. p. 275–282.
- Fortier, R., M. Allard, and M.-K. Seguin. 1994. Effect of physical properties of frozen ground on electrical resistivity logging. *Cold Reg. Sci. Technol.* 22:361–384. doi:10.1016/0165-232X(94)90021-3
- Fortier, R., A.-M. LeBlanc, M. Allard, S. Buteau, and F. Calmels. 2008. Internal structure and conditions of permafrost mounds at Umiujaq in Nunavik, Canada, inferred from field investigation and electrical resistivity tomography. *Can. J. Earth Sci.* 45:367–387. doi:10.1139/E08-004
- French, H.K., A. Binley, I. Kharkhordin, B. Kulesa, and S.S. Krylov. 2006. Cold regions hydrogeophysics: Physical characterisation and monitoring. In: H. Vereecken et al., editors, *Applied hydrogeophysics*. Springer, Dordrecht, the Netherlands. p. 195–232.
- Grahame, D.C. 1947. The electrical double layer and the theory of electrocapilarity. *Chem. Rev.* 41:441–501. doi:10.1021/cr60130a002
- Gränicher, H., C. Jaccard, P. Scherrer, and A. Steinemann. 1957. Dielectric relaxation and the electrical conductivity of ice crystals. *Discuss. Faraday Soc.* 23:50–62. doi:10.1039/df9572300050
- Grimm, R.E., D.E. Stillman, S.F. Dec, and M.A. Bullock. 2008. Low-frequency electrical properties of polycrystalline saline ice and salt hydrates. *J. Phys. Chem. B* 112:15,382–15,390. doi:10.1021/jp8055366
- Gruen, D.W., and S. Marcelja. 1983. Spatially varying polarization in ice. *J. Chem. Soc. Faraday Trans. 2* 79:211–223. doi:10.1039/f29837900211
- Hall, D.L., S.M. Sterner, and R.J. Bodnar. 1988. Freezing point depression of NaCl-KCl-H₂O solutions. *Econ. Geol.* 83:197–202. doi:10.2113/gsecon-geo.83.1.197
- Han, L., A. Tsunekawa, and M. Tsubo. 2010. Monitoring near-surface soil freeze-thaw cycles in northern China and Mongolia from 1998 to 2007. *Int. J. Appl. Earth Obs. Geoinf.* 12:375–384. doi:10.1016/j.jag.2010.04.009
- Hauck, C., M. Böttcher, and H. Maurer. 2010. A new model for quantifying subsurface ice content based on geophysical datasets. *The Cryosphere Discuss* 4:787–821. doi:10.5194/tcd-4-787-2010
- Hayley, K., L.R. Bentley, M. Gharibi, and M. Nightingale. 2007. Low temperature dependence of electrical resistivity: Implications for near surface geophysical monitoring. *Geophys. Res. Lett.* 34:L18402. doi:10.1029/2007GL031124
- Hilbich, C., C. Hauck, M. Hoelzle, M. Scherler, L. Schudel, I. Völksch, D. Vonder Mühl, and R. Mäusbacher. 2008. Monitoring mountain permafrost evolution using electrical resistivity tomography: A 7-year study of seasonal, annual, and long-term variations at Schilthorn, Swiss Alps. *J. Geophys. Res.* 113:F01S90. doi:10.1029/2007JF000799
- Hoekstra, P., P.V. Sellman, and A.J. Delaney. 1974. Airborne resistivity mapping of permafrost near Fairbanks, Alaska. *Geophysics* 40:641–656.
- Hubbard, S.S., C. Gangodagamage, B. Dafflon, H. Wainwright, J. Peterson, A. Gusmeroli, Y. Wu, J. Doetsch, J.E. Peterson, C. Wilson, C. Tweedie, and S.D. Wulfschleger. 2012. Quantifying and relating subsurface and land-surface variability in permafrost environments using surface geophysical and LiDAR datasets. *Hydrogeology J.* (In press).
- Jones, D.P. 2002. Investigation of clay-organic reactions using complex resistivity. MS thesis. Colorado School of Mines, Golden.
- Kemna, A. 2000. Tomographic inversion of complex resistivity-theory and application. Der Andere Verlag, Osnabrück, Germany.
- Kimball, J.S., K.C. McDonald, S. Frolking, and S.W. Running. 2004. Radar remote sensing of the spring thaw transition across a boreal landscape. *Remote Sens. Environ.* 89:163–175. doi:10.1016/j.rse.2002.06.004
- Kneisel, C., C. Hauck, R. Fortier, and B. Moorman. 2008. Advances in geophysical methods for permafrost investigations. *Permafrost Periglacial Processes* 19:157–178. doi:10.1002/ppp.616
- Krautblatter, M., and C. Hauck. 2007. Electrical resistivity tomography monitoring of permafrost in solid rock walls. *J. Geophys. Res.* 112:F02S20. doi:10.1029/2006JF000546
- Krautblatter, M., and N. Zisser. 2012. Laboratory evidence for linear temperature-resistivity pathways of thawed, supercooled and frozen permafrost rocks. *Geophys. Res. Lett.* (In press).
- Krautblatter, M., S. Verleysdonk, A. Flores-Orozco, and A. Kemna. 2010. Temperature-calibrated imaging of seasonal changes in permafrost rock walls by quantitative electrical resistivity tomography (Zugspitze, German/Austrian Alps). *J. Geophys. Res.* 115:F02003. doi:10.1029/2008JF001209
- Lashof, D.A., and D.R. Ahuja. 1990. Relative contributions of greenhouse gas emissions to global warming. *Nature* 344:529–532. doi:10.1038/344529a0
- Lesmes, D.P., and S.P. Friedman. 2005. Relationships between the electrical and hydrogeological properties of rocks and soils. In: Y. Rubin and S. Hubbard, editors, *Hydrogeophysics*. Springer, Dordrecht, the Netherlands. p. 87–128.
- Lesmes, D.P., and F.D. Morgan. 2001. Dielectric spectroscopy of sedimentary rocks. *J. Geophys. Res.* 106:13,329–13,346. doi:10.1029/2000JB900402
- Low, P.F., D.M. Anderson, and P. Hoekstra. 1968. Some thermodynamic relationships for soils at or below the freezing point: 1. Freezing point depression and heat capacity. *Water Resour. Res.* 4:379–394. doi:10.1029/WR004i002p00379
- McGinnis, L.D., K. Nakao, and C.C. Clark. 1973. Geophysical identification of frozen and unfrozen ground, Antarctica. In: Permafrost: North American Contribution Second International Permafrost Conference, Yakutsk, Russia. 13–28 July 1973. Natl. Acad. of Sci., Washington, DC. p. 136–146.
- Morley, C.R., J.A. Trofymow, D.C. Coleman, and C. Cambardella. 1983. Effects of freeze-thaw stress on bacterial populations in soil microcosms. *Microb. Ecol.* 9:329–340. doi:10.1007/BF02019022
- Mühl, D.V., C. Hauck, and H. Gubler. 2002. Mapping of mountain permafrost using geophysical methods. *Prog. Phys. Geogr.* 26:643–660. doi:10.1191/0309133302pp356ra
- Murrmann, R.P. 1973. Ionic mobility in permafrost. In: Permafrost: North American Contribution Second International Permafrost Conference, Yakutsk, Russia. 13–28 July 1973. Natl. Acad. of Sci., Washington, DC. p. 352–359.
- Olhoeft, G.R. 1977. Electrical properties of natural clay permafrost. *Can. J. Earth Sci.* 14:16–24. doi:10.1139/e77-002
- Olhoeft, G.R. 1985. Low-frequency electrical properties. *Geophysics* 50:2492–2503.
- Panikov, N.S. 2009. Microbial activity in frozen soils. In: R. Margesin, editor, *Permafrost soils*. Springer-Verlag, Berlin. p. 119–147.

- Pelton, W.H., W.R. Sill, and B.D. Smith. 1978. Interpretation of complex resistivity and dielectric data. Part I. *Geophys. Trans.* 29:297–330.
- Penner, E. 1970. Thermal conductivity of frozen soils. *Can. J. Earth Sci.* 7:982–987. doi:10.1139/e70-091
- Revil, A. 2012. Spectral induced polarization of shaly sands: Influence of the electrical double layer. *Water Resour. Res.* 48:W02517. doi:10.1029/2011WR011260
- Revil, A., and N. Florsch. 2010. Determination of permeability from spectral induced polarization in granular media. *Geophys. J. Int.* 181:1480–1498.
- Revil, A., K. Koch, and K. Holliger. 2012. Is it the grain size or the characteristic pore size that controls the induced polarization relaxation time of clean sands and sandstones? *Water Resour. Res.* 48:W05602. doi:10.1029/2011WR011561
- Rubin, Y., and S. Hubbard, editors. 2005. *Hydrogeophysics*. Springer, Dordrecht, the Netherlands.
- Running, S.W., J.B. Way, K.C. McDonald, J.S. Kimball, S. Frolking, A.R. Keyser, and R. Zimmerman. 1999. Radar remote sensing proposed for monitoring freeze–thaw transitions in boreal regions. *Eos Trans. AGU* 80(19): 213. doi:10.1029/99EO00158
- Schön, J.H. 1996. *Physical properties of rocks: Fundamentals and principles of petrophysics*. Pergamon, Oxford, UK.
- Schuur, E.A.G., and B. Abbott. 2011. Climate change: High risk of permafrost thaw. *Nature* 480:32–33. doi:10.1038/480032a
- Schuur, E.A.G., J.G. Vogel, K.G. Crummer, H. Lee, J.O. Sickman, and T.E. Osterkamp. 2009. The effect of permafrost thaw on old carbon release and net carbon exchange from tundra. *Nature* 459:556–559. doi:10.1038/nature08031
- Scott, J., and R. Baker. 2003. Determining pore-throat size in permo-triassic sandstones from low-frequency electrical spectroscopy. *Geophys. Res. Lett.* 30(9):1450. doi:10.1029/2003GL016951
- Sellmann, P.V. 1975. The classification and geomorphic implication of thaw lakes on the Arctic Coastal Plain, Alaska. U.S. Army CRREL Res. Rep. 344. U.S. Army Cold Reg. Res. Eng. Lab, Hanover, NH.
- Sharma, S., Z. Szele, R. Schilling, J.C. Munch, and M. Schloter. 2006. Influence of freeze–thaw stress on the structure and function of microbial communities and denitrifying populations in soil. *Appl. Environ. Microbiol.* 72:2148–2154. doi:10.1128/AEM.72.3.2148-2154.2006
- Shiklomanov, N.I., D.A. Streletskiy, F.E. Nelson, R.D. Hollister, V.E. Romanovsky, C.E. Tweedie, J. G. Bockheim, and J. Brown. 2010. Decadal variations of active-layer thickness in moisture-controlled landscapes, Barrow, Alaska. *J. Geophys. Res.* 115:G00104. doi:10.1029/2009JG001248
- Sidorova, M.P., and D.A. Fridrikhsberg. 1973. Study of the induced polarization of systems simulating soils during freezing. In: *Permafrost: North American Contribution Second International Permafrost Conference, Yakutsk, Russia. 13–28 July 1973*. Natl. Acad. of Sci., Washington, DC. p. 347–349.
- Slater, L. 2007. Near surface electrical characterization of hydraulic conductivity: From petrophysical properties to aquifer geometries—A review. *Surv. Geophys.* 28:169–197. doi:10.1007/s10712-007-9022-y
- Slater, L., D. Ntarlagiannis, and D.N. Wishart. 2006. On the relationship between induced polarization and surface area in metal-sand and clay-sand mixtures. *Geophysics* 71:A1–A5.
- Stahli, M., and D. Stadler. 1997. Measurement of water and solute dynamics in freezing soil columns with time domain reflectometry. *J. Hydrol.* 195:352–369. doi:10.1016/S0022-1694(96)03227-1
- Steponkus, P.L., and D. Lynch. 1989. Freeze/thaw-induced destabilization of the plasma membrane and the effects of cold acclimation. *J. Bioenerg. Biomembr.* 21:21–41. doi:10.1007/BF00762210
- Stillman, D.E., R.E. Grimm, and S.F. Dec. 2010. Low-frequency electrical properties of ice-silicate mixtures. *J. Phys. Chem. B* 114:6065–6073. doi:10.1021/jp9070778
- Sumner, J.S. 1976. *Principles of induced polarization for geophysical exploration*. Elsevier, Amsterdam.
- Tarnocai, C., E.A.G. Schuur, P. Kuhry, G. Mazhitova, and S. Zimov. 2009. Soil organic carbon pools in the northern circumpolar permafrost region. *Global Biogeochem. Cycles* 23:GB2023. doi:10.1029/2008GB003327
- Tong, M., and H. Tao. 2007. Experimental study of induced polarization relaxation time spectra of shaly sands. *J. Petrol. Sci. Eng.* 59:239–249. doi:10.1016/j.petrol.2007.04.004
- Vanhala, H., P. Lintinen, and A. Ojala. 2009. Electrical resistivity study of permafrost on Ridnišohkka fell in northwest Lapland, Finland. *Geophysica* 45:103–118.
- von Hippel, A. 1988. The dielectric relaxation spectra of water, ice, and aqueous solutions, and their interpret at ion 1. Critical survey of the status-quo for water. *IEEE Trans. Electr. Insul.* 23:801–816. doi:10.1109/14.8745
- Wang, D., Y. Zhu, W. Ma, and Y. Niu. 2006. Application of ultrasonic technology for physical–mechanical properties of frozen soils. *Cold Reg. Sci. Technol.* 44:12–19. doi:10.1016/j.coldregions.2005.06.003
- Watanabe, K., and M. Ito. 2008. In situ observation of the distribution and activity of microorganisms in frozen soil. *Cold Reg. Sci. Technol.* 54:1–6. doi:10.1016/j.coldregions.2007.12.004
- Watanabe, K., and M. Mizoguchi. 2002. Amount of unfrozen water in frozen porous media saturated with solution. *Cold Reg. Sci. Technol.* 34:103–110. doi:10.1016/S0165-232X(01)00063-5
- Weller, A., L. Slater, S. Nordsiek, and D. Ntarlagiannis. 2010. On the estimation of specific surface per unit pore volume from induced polarization: A robust empirical relation fits multiple data sets. *Geophysics* 75:WA105–WA112. doi:10.1190/1.3471577
- Williams, K.H., A. Kemna, M.J. Wilkins, J. Druhan, E. Arntzen, A. Lucie N’Guessan, P.E. Long, S.S. Hubbard, and J.F. Banfield. 2009. Geophysical monitoring of coupled microbial and geochemical processes during stimulated subsurface bioremediation. *Environ. Sci. Technol.* 43(17): 6717–6722. doi:10.1021/es900855j
- Wong, J. 1979. An electrochemical model of the induced-polarization phenomenon in disseminated sulfide ores. *Geophysics* 44:1245–1265. doi:10.1190/1.1441005
- Yoshikawa, K., C. Leuschen, A. Ikeda, K. Harada, P. Gogineni, P. Hoekstra, L. Hinzman, Y. Sawada, and N. Matsuoka. 2006. Comparison of geophysical investigations for detection of massive ground ice (pingo ice). *J. Geophys. Res.* 111:E06S19. doi:10.1029/2005JE002573
- Zhang, T., R.G. Barry, and R.L. Armstrong. 2004. Application of satellite remote sensing techniques to frozen ground studies. *Polar Geogr.* 28:163–196. doi:10.1080/789610186
- Zimov, S., E.A.G. Schuur, and F. Stuart Chapin III. 2006. Permafrost and the global carbon budget. *Science* 312:1612–1613. doi:10.1126/science.1128908
- Zisser, N., and A. Kemna. 2010. Dependence of spectral-induced polarization response of sandstone on temperature and its relevance to permeability estimation. *J. Geophys. Res.* 115:B09214. doi:10.1029/2010JB007526